Wood Defect Classification Based on Two-Dimensional Histogram Constituted by LBP and Local Binary Differential Excitation Pattern

SHAOLI LI[1,2], **DEJIAN LI**[1,2], **AND WEIQI YUAN**[1]

[1]Computer Vision Group, Shenyang University of Technology, Shenyang 110870, China
[2]School of Electrical Engineering, Shenyang University of Technology, Shenyang 110870, China

Corresponding author: Shaoli Li (lishaoli@sut.edu.cn)

ABSTRACT A classification algorithm based on LBP and local binary differential excitation pattern is presented for the classification of the crack and the linear mineral line on the surface of the birch veneer. The local binary differential excitation pattern (LB_DEP) is a texture description model proposed in this paper, which is generated by the combination of LBP and Weber's Law and describes the incidence relation between the image texture and the human visual perception. And the feature extracted by LB_DEP is expressed in a one-dimensional histogram. Then we establish a two-dimensional (2D) histogram constituted by the one-dimensional (1D) histogram of LBP and LB_DEP after being normalized and consolidated. Finally, the 2D histogram is used to classify the defects with Euclidean distance classifier. In addition, we establish an automatic optical inspection system for the birch ice cream bar. We also conduct the experiments with the images captured by the system. The results demonstrate that, compared with the state-of-the-art methods, our proposed algorithm can provide a better classification effect for the crack and the mineral line—the *Recall*, *Precision* and *FNR* are 0.930, 0.943 and 0.070 respectively. And the time consumption is 0.1416 s, which belongs to the millisecond level as with the compared methods.

INDEX TERMS Automatic optical inspection, defect detection, wood, LBP, Weber's Law, crack.

I. INTRODUCTION

Wood strength plays an important role in the wood products. And wood defects, especially crack defects will have an adverse impact on wood strength. Crack is a serious defect on the wood surface, which changes the physical structure of the wood, affects wood's mechanical properties, damages the toughness and impact resistance of the wood, and endangers the quality, safety and service life of the wood products seriously. So the detection of the crack becomes the most important content in the area of wood defect detection. The ice cream bar is a common and widely used wood product, which is the handle of ice cream and often made up of birch. The structure of an ice cream bar is shown in Fig. 1, which is a rectangular wood veneer. The production process

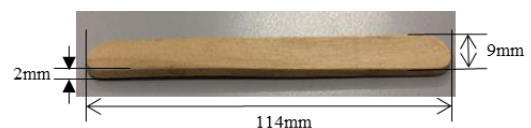The associate editor coordinating the review of this manuscript and approving it for publication was Md. Asikuzzaman.

FIGURE 1. Birch ice cream bar and its dimensions.

of the ice cream bar needs to go through cooking, peeling, rotary cutting and punching. However, during the process of punching, the veneer might be torn by the blunt force resulted from the not sharp enough punching knife and the inappropriate location of the veneer obtained from the previous rotary cutting process. And the tear caused by blunt force would lead to the ice cream bar generating crack defect. Among the generated cracks, most of them close tightly at the gap and present dark and thin lines, which is very similar to the mineral line defect generated during the birch's growth, as shown in Fig. 2. However, the crack defect of the ice cream

FIGURE 2. Crack and mineral line on the surface of the birch veneer: (a) Crack and (b) Mineral line.

bar is very easy to scratch the user's mouth and tongue, so it needs to be detected and eliminated strictly. And the mineral line defect belongs to the natural texture of the wood, which will only affect the aesthetics. Thus, the mineral line defect is usually ignored. Therefore, if the crack is wrongly identified as a mineral line, the ice cream bar with the crack might cause the personal injury during use. Conversely, if the mineral line is wrongly identified as a crack, the corresponding product individual will be eliminated, which causes the waste of the timber resources. Therefore, it has been an important work to distinguish the crack and the mineral line before the ice cream bars are put into the market.

At present, most of the wood defect inspection and classification tasks, including the classification of the crack and the mineral line of the ice cream bars are implemented by the trained human technicians. However, this inspection approach will fatigue the eye of the observers, which may lead to lower efficiency and reliability of the defect detection result. Therefore, the automatic methods of wood nondestructive testing are developed gradually. The wood nondestructive testing methods could be divided into two categories: the visual testing and the non-visual testing. The visual testing methods acquire the wood images by the infrared thermal imaging [1], the X-ray imaging [2] or the visible light imaging [3], and then the defects are detected through digital image processing technology. The non-visual testing methods detect the changes of the relevant parameters of the radar wave, the ultrasonic wave or the pressure wave before and after they penetrate the wood [4], [5]. And the defect types are identified by analyzing the characteristics of the relevant parameters. Among the wood nondestructive testing methods mentioned above, the visual testing method based on visible light has become one of the most widely used methods in the field of wood defect detection due to the advantages of convenience, high repeatability and low price. However, the crack and the mineral line of the ice cream bar are very similar in many aspects of the image features such as geometric shape, grayscale and color. And both of the defects are the elongated strips and extending in the direction of the wood fiber's extension. Moreover, both of them have a low grayscale relative to the general veneer surface. All the above make it hard to classify these two wood defects based on the current methods of machine vision.

Therefore, to classify the crack defects and the mineral line defects on the surface of birch veneer, a 2D histogram method based on LBP and LB_DEP is proposed in this paper. The proposed method is as follows: First, OTSU, mean filtering, image subtraction and geometric parameter

constraint are used to segment the potential defect areas. Second, a new image texture description method named LB_DEP is proposed based on LBP and differential excitation (DE). LB_DEP reflects the correlation between the location of the different textures and the DE of the human visual perception of an image. Then, the LBP histogram and the LB_DEP histogram are consolidated to generate a 2D histogram. Finally, the defects are identified by the matching result of the target 2D histogram and the reference 2D histogram with Euclidean distance classifier.

This paper is organized as follows: Section II introduces the relevant work. Section III presents the experimental equipment and the image data set. Section IV presents the detailed methods of the defects classification. The experiments and results are detailed in section V. We conclude the paper in section VI.

II. RELATED WORK
The related work is presented from two perspectives. First, from the perspective of the research object, that is, wood crack and mineral line. Second, from the perspective of mathematical theory.

A. RELATED WORK ON WOOD CRACK AND MINERAL LINE CLASSIFICATION
At present, many researchers have studied the wood crack defect detection a lot based on visible light machine vision [6]. However, few methods have been published to distinguish the cracks and the mineral lines. And most attention has been focused on the detection of the cracks, and the classification of the cracks and other defects with obvious interclass characteristics. For example, in [7], the author uses the PCA and compressive sensing methods to identify cracks, live knots and dead knots. Multidimensional feature vectors [8] including the geometric feature, the texture feature and the invariant moment feature are extracted for training. In [9], the author proposes the method of using linear discriminant analysis and compressive sensing to identify cracks, live knots and dead knots on the basis of [7] and [8]. Chang et al. smooth image with the convex optimization method, and then segment the defect areas using the Otsu algorithm. Then the multidimensional features of geometry and color are extracted as the input of the classifier, so as to realize the detection and classification of the cracks and the three kinds of knot defects [10]. In [11], the author proposes an unsupervised clustering method for the identification of insect eyes, knots, cracks, discolorations and decays. The moments of order 1, order 2, and order 3 of the wood veneer images in R, G, and B color spaces are extracted respectively. Then the algorithm of k-means is used to cluster the feature data sets to identify the defects. Unfortunately, this method only works well for the knots, and the recall rate of other defects is only 57.1%. Consequently, the author proposes a method replacing the feature of color moments with the five typical features of the gray co-occurrence matrix in 2010 [12]. And for the detection of knots and cracks, MM Hittawe

proposes a classification and detection method that extracts the LBP features and the SURF features and inputs them to SVM classifier [13].

In addition, a few researches have studied the classification problem of the cracks and the mineral lines, but the closed and dark linear cracks have not been considered. For example, reference [14] proposes the S-LVQ network method for the classification of 11 defects such as cracks and mineral lines, and a total of 17 gray features are extracted as the input of the S-LVQ classifier. But only the serious cracks which appear as a bright white region generated by the light transmitting from the top surface to the bottom surface of the veneer gap are considered. And the tightly closed cracks which appear as a dark and thin line are not considered [15], [16]. In [17], the author proposes a feed-forward artificial neural network for the detection of the 11 kinds of defects mentioned in [15]. So the problem that the tightly closed cracks are not considered still remains to be resolved.

Our research group has studied the detection and recognition method of the surface defects of the birch ice cream bar since 2015. For the classification of the tightly closed cracks and the mineral lines, some researches have been implemented. At present, the methods proposed are included in the [18], [19]. In [18], a method based on the sub-region variable-scale Gaussian fitting is proposed, which fits each transverse section of the defect area into a Gaussian curve, and uses the parameters of the Gaussian curve as the characteristic elements of the classification. However, some information is lost in the process of the Gaussian fitting, which weakens the ability of the feature expression and the accuracy of the classification consequently. In [19], a method based on the feature fusion of the texture ridges is proposed, and the fluctuation degree of the ridges in the direction of the texture's extension is extracted to classify the defects. But, the extracted ridge line is a single pixel wide line, and the shape of the line is easily affected by noise, which affects the accuracy of the classification.

In summary, the current researches do not pay attention to the classification of the tightly closed dark cracks and the mineral lines. Alternatively, the focus is on the detection of the dark cracks, the classification of the defects with large differences such as the cracks and the knots, and the classification of the white and transparent cracks and the mineral lines. Moreover, the method proposed by our research group in the early stage still needs to be improved in the accuracy of the classification.

B. RELATED WORK ON THEORIES OF LBP AND DIFFERENTIAL EXCITATION

LBP is a popular image texture feature representation algorithm, and the basic idea is as follows [20], [21]. First, a local neighborhood with P as the number of sampling points and R as the radius is selected around a certain central point and expressed as (P, R). Then, the gray value of the center point is taken as the threshold value, and the gray value of each point in the neighborhood is compared with the threshold value.

Finally, binary processing and binary coding are carried out. Then the obtained coding value is the LBP value of the central point, and the equation is as follows:

$$LBP_{P,R}(x_c, y_c) = \sum_{i=0}^{P-1} 2^i \cdot s(g_i - g_c) \quad (1)$$

$$s(g_i - g_c) = \begin{cases} 1, g_i - g_c \geq 0 \\ 0, g_i - g_c < 0 \end{cases} \quad (2)$$

where (x_c, y_c) is the coordinate of the center point c, g_c is the gray value of point c, g_i is the gray value of the point in the neighborhood, and i is the serial number of the points in the neighborhood. R is the radius of the neighborhood, and P is the number of pixels in the neighborhood within radius R. For a texture patch, the value of $LBP_{P,R}$ is usually taken as the horizontal coordinate and the number of pixels with corresponding $LBP_{P,R}$ value is taken as the vertical coordinate to form a one-dimensional histogram to express the texture state of the patch, which has been widely used in various fields of digital image processing, including wood defect detection and recognition. In [22], LBP histogram is utilized in the detection of the knot defects on the wood edges. First, the image is divided into many small patches, and then LBP histogram is used to extract the texture features. Next, the extracted LBP histograms are regarded as the criterion to classify the defect and noise. Reference [23] classifies the CT images of six broadleaf trees with the feature vector of LBP histogram. Then in [24], the similar usage of LBP is utilized to detect surface defects of the bamboo veneers, and obtains a good result. Inspired by the successful application of LBP in wood defect detection, this paper applies it to the classification of the cracks and the mineral lines of birch veneer.

As the final recipient of images, human eyes have the ability to distinguish the objects very similar to each other. Therefore, the proper use of the human visual characteristics can help to obtain a more efficient texture classifier. There is a psychophysical law that the human vision is not sensitive to the absolute sensory stimuli, but sensitive to the relative stimuli, which is exactly described by Weber's law [25], [26]. Based on the Weber's law, a physical quantity used to describe the human eyes' perception of the image—differential excitation (DE) [27], [28] is defined as follows:

$$\xi(x_c) = \arctan \left[\alpha \cdot \frac{\sum_{i=0}^{Q-1} (x_i - x_c)}{\max(I) - \min(I)} \right] \quad (3)$$

where x_c is the gray value of the current pixel, x_i is the gray value of the neighboring pixel of x_c, $\xi(x_c)$ is the DE value of pixel x_c, and I is the input image. And α is a parameter introduced to prevent the arctangent function changing too fast, and meanwhile to simulate the nonlinear characteristics of the human eyes. According to [29], α is set to 5. Q represents the pattern parameter.

As an image feature descriptor, differential excitation is often used in combination with the existing digital image processing methods, among which LBP is one of the most common algorithms combined with differential excitation. The combinative modes of LBP and differential excitation can be divided into two types. One is improving LBP algorithm by using differential excitation, so as to effectively enhance the information extracted by LBP. And the representative researches of this type mainly include [30], [31], and [32]. Another type is integrating LBP and differential excitation, that is, introducing the visual perception information expressed by differential excitation as a new dimension to improve the effect of image representation, feature extraction, or pattern recognition. And the representative researches include [33], [30], and [35]. The specific methods of each representative research are as follows. In [30] and [31], the differential excitation is applied to improve LBP algorithm. It changes the absolute ratio of the grayscale of pixel x_i in the neighborhood and the target pixel x_c into a constant value, and compares it with the relative value $|x_i\text{-}x_c|/x_c$, so as to execute the binary coding of LBP. Reference [32] proposes a threshold value determination method based on differential excitation, in which the threshold value is composed of the sum of two parts values. The first part is the sum of the difference value between the gray value of the target pixel and its neighboring pixels, and the second part is the gray value of the target pixel. Then the threshold value is used as the reference threshold of binaryzation in LBP algorithm. In [33], for measuring the degree of image degradation, the differential excitation image is first obtained according to (3) above, and the gradient image of the differential excitation is obtained according to anisotropy. Then, differential excitation is quantified to obtain the differential quantization image, which is weighted fused with differential excitation image and gradient image respectively. And the statistical characteristic values obtained are used for image quality evaluation. In [34], the differential excitation image is still obtained according to (3), and then it is quantified and fused with LBP image, so as to obtain a set of two-dimensional eigenvectors for image description. In [35], aiming at palmprint recognition, Gabor filter is first utilized to conduct linear filtering on palmprint images to generate directional and energy images. Then the differential excitation image is generated by the differential excitation filtering of the energy map. Finally, the direction image and the differential excitation image are quantized on average to construct the histogram of line Weber features, and the better recognition effect is acquired. According to the relevant references, the combination of LBP and differential excitation achieves better effects in the corresponding problems.

Inspired by the availability of the combination of LBP and differential excitation, we introduce it to the problem of classifying the tightly closed dark cracks and the mineral lines on the surface of the birch veneer. We present a mapping model that integrates LBP and differential excitation to generate a one-dimensional histogram which reflects the relationship of
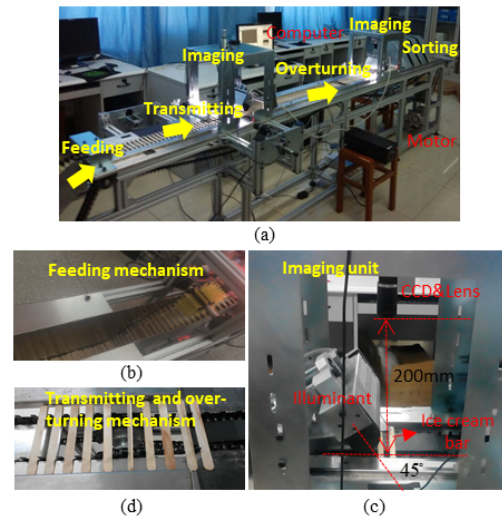
FIGURE 3. Ice cream bar imaging equipment: (a) The overall structure of the imaging equipment and the basic process of imaging, (b) Feeding mechanism of the transmission unit, (c) Structure of the imaging unit, (d) Transmitting and overturning mechanism of the transmission unit.

the textures and the DE on the image. Then we combine the generated one-dimensional histogram with LBP histogram to constitute a 2D histogram to describe the texture features of the images. Finally, the defects are classified with Euclidean distance classifier and the generated 2D histogram.

III. BIRCH ICE CREAM BAR IMAGING EQUIPMENT AND IMAGE DATA SET
A. IMAGING EQUIPMENT AND IMAGING APPROACH OF THE BIRCH ICE CREAM BAR
In this research, the ice cream bar processed from the birch is taken as the experimental object. The length, width, and thickness of the wood veneer are 114 mm, 9.6 mm, and 2 mm respectively. And the two ends of the ice cream bar are arc-shaped, as shown in Fig. 1.

We first construct an imaging equipment for the detection of the ice cream bar defects. As shown in Fig. 3, the equipment is mainly composed of four units: transmission unit, imaging unit (two groups), data processing unit and sorting unit. In Fig 3-(a), the movement route of the ice cream bar is marked by the yellow arrows. The imaging process is as follows. First, the ice cream bars are added to the chain track in sequence by the feeding mechanism (as shown in Fig. 3-(b)) of the transmission unit, and then they are transferred forward under the drive of the motor (Model: YS-7124). Then the camera is triggered by the photoelectric switch to acquire an image while the ice cream bar is transported to the area of the first imaging unit (as shown in Fig. 3-(c)). Next, the ice cream bar passes through the turnover mechanism (as shown in Fig. 3-(d)), where the upper and the lower surfaces of the ice cream bar are switched. Consequently, the image of the opposite surface of the ice cream bar is captured while the ice cream bar moves to the next imaging unit. So far, the images of the upper and the lower surfaces of the ice cream bar are captured. The images are stored in the computer connected to
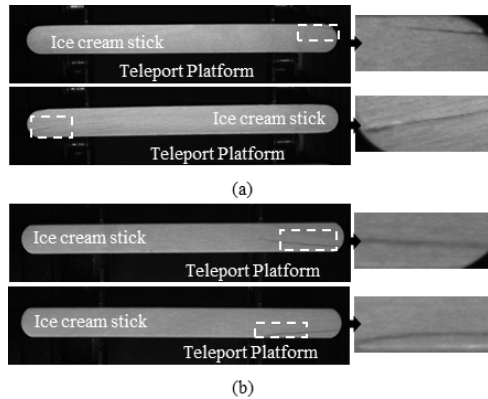
FIGURE 4. Images in the data set: (a) Ice cream bar with cracks and (b) Ice cream bar with mineral lines.

the imaging equipment. Finally, the automatic sorting unit is controlled to sort the ice cream bars according to the defect recognition re- sults of the computer. And the sorting process is realized by the electromagnetic injection valve (Model: MAC 117B-501BAAA).

Furthermore, in the imaging unit, the camera is a XIME MQ013MG-E2 and contains 1280 × 1024 active pixels. The lens is a Computar MT1214-MP2. The illuminant is a high uniform strip white light source of OPT. As shown in Fig. 3-(c), the camera is installed 200 mm above the ice cream bar, and the illuminant is located at the upper left of the ice cream bar with a light angle of incidence of 45°. In this paper, the imaging resolution of the camera is set to 1280 × 256, and the working mode is set to the trigger shooting mode.

B. IMAGE DATA SET

The ice cream bars with cracks and mineral lines are sorted out by the technicians, and the total number of these two kinds of samples is 134 and 177 respectively. The upper and lower surfaces of these samples contain 241 cracks and 202 mineral lines. Then, the image data set with the size of 443 is established with the two reverse surface images of the ice cream bar samples. Fig. 4 is the examples of the image captured by the equipment of Fig. 3.

IV. WOOD DEFECT CLASSIFICATION METHOD BASED ON 2D HISTOGRAM CONSTITUTED BY LBP AND LB_DEP

In this section, we present a classification method based on the 2D histogram constituted by LBP and local binary differential excitation pattern for the cracks and the mineral lines. The local binary differential excitation pattern (LB_DEP) is a new model proposed in this paper to describe the image texture, which is through a way of mapping to generate a one-dimensional histogram integrating the location of the image texture information and the human visual perception information. The proposed classification method of the cracks and the mineral lines mainly consists of three parts: linear defect area segmentation, feature extraction and feature histogram generation, and defect classification. The overall
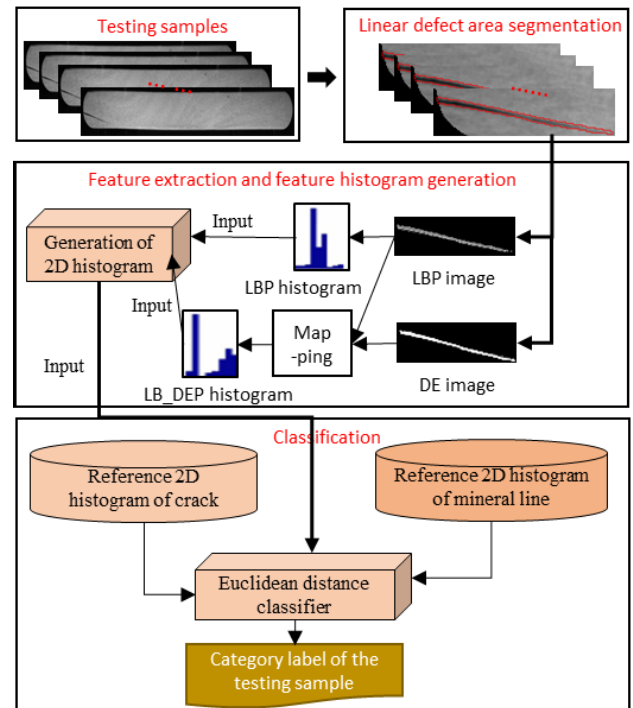
FIGURE 5. Overview of the proposed wood defects classification method.

flow of this method is shown in Fig. 5, and the details are presented in the following sections.

A. LINEAR DEFECT AREA SEGMENTATION

Before classifying, some image preprocessing methods are applied to segmentation of the crack and the mineral line areas.

As the ice cream bar shows the obvious bright intensity area in the image, it can be easily located by the OTSU [36] algorithm. Then, the defect area is segmented by

$$I_t(x, y) = \begin{cases} 255, & \bar{I}(x, y) - I(x, y) > T \\ 0, & \bar{I}(x, y) - I(x, y) \leq T \end{cases} \tag{4}$$

where I_t is the image after marking the defect area, I is the input image to be processed, $\bar{I}$ represents the image I after mean filtering with a 10 × 10 template, and T is the threshold whose value is obtained through the observation and the statistics of the samples in the data set. And (x, y) represents the coordinates of the image-pixel. $I_t(x, y), I(x, y)$, and $\bar{I}(x, y)$ represent the value of (x,y) in the image I_t, I and $\bar{I}$ respectively.

Furthermore, the crack and the mineral line areas are detected by screening with a pre-set threshold T_a to remove some of the smaller noises from the segmented defect areas by (4). However, some false defects are also produced, and the areas of the false defects have the similar gray intensity with the real defect areas in the image. Unlike other defects, the cracks and mineral lines are linear, so they can be distinguished from the false defect areas with the condition
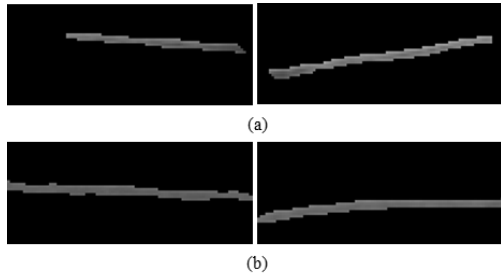
FIGURE 6. Defect segmentation effect of image in Fig. 4: (a) Cracks and (b) Mineral lines.
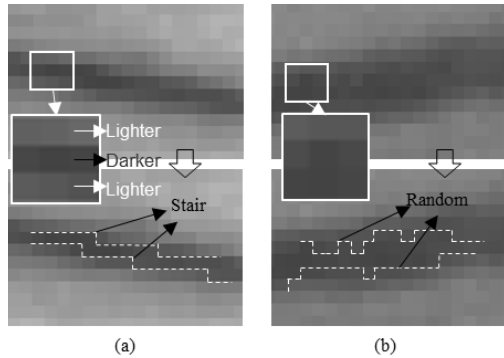

FIGURE 7. Texture of the crack and the mineral line: (a) Ladder texture of the crack and (b) Random texture of the mineral line.

that the aspect ratio of their minimum external rectangle is greater than a certain threshold T_r. The specific values of T_a and T_r are obtained through the observation and statistics of the experiment. Finally, the segmentation effect of the linear region is shown in Fig. 6.

B. FEATURE EXTRACTION

In this section, we extract the features of the segmented linear defect area and use them in the following classification to identify the defects. The features extracted in this research are based on LBP and LB_DEP. LB_DEP is an image feature description model we proposed based on the combination of LBP and human visual sensory characteristics. The details are described as follows.

1) DEFECT CLASSIFICATION BASED ON LBP

The cracks and the mineral lines of the birch veneer have completely different generating causes. The crack is generated by the wood fiber cluster's tear along the longitudinal direction, and the texture arrangement presents a certain rule, as shown in Fig. 7-(a), which is similar to a ladder. In contrast, the mineral line is generated by the mineral deposition during the growth of the birch, and the distribution of the pigment depth is random to a certain extent, as shown in Fig. 7-(b). It can be seen in Fig. 7, there is a certain difference in the texture styles between the cracks and the mineral lines. Therefore, LBP which is an image texture description method, can be used and achieve a considerable distinguish effect theoretically. So we conduct an experiment. First, the LBP

histogram of the defect area to be identified is obtained, and then the similarity between it and the target texture reference histogram is measured by chi-square distance [37]. Since the relevant theory and experimental methods of LBP are quite mature, the specific details are not repeated here. For details, please refer to [38], and [39].

A point worth explaining is that the "target texture reference histogram" mentioned above is established according to the samples in the training data set. Taking the reference histogram $H_c(LBP)$ of the cracks as an example, the specific established method is as follows:

$$H_c(LBP) = \frac{1}{n} \sum_{i=1}^{n} H(t_i) \tag{5}$$

where i is the sequence number of the samples in the training data set, n is the total number of the cracks in the training data set, and $H(t_i)$ is the LBP value of the i'th crack sample LBP histogram at the horizontal coordinate t. The reference histogram $H_m(LBP)$ of the mineral line is established as $H_c(LBP)$.

The specific experimental data and results of this section detail in section V below.

2) LOCAL BINARY DIFFERENTIAL EXCITATION PATTERN (LB_DEP)

According to the experimental results of section V, the evaluation index *Recall* and *Precision* of the classification of the cracks and the mineral lines based on LBP are 0.878 and 0.915, respectively. It can be said that this is a good effect, but there are still about 12% of the images misjudged, especially the mineral line, whose the ratio of misjudgments is about 17%. In order to improve the accuracy of the classification, differential excitation (DE) which describes the visual and sensory features of human eyes is introduced. At present, the current image feature extraction and expression methods based on differential excitation have been successfully applied to the image quality assessment [40], [41], the medical image processing (e.g., vascular image enhancement [42], colon polyps texture description [43]), the biometric identification (e.g., facial expression recognition[44], palmprint recognition [35]), and other fields. Inspired by the successfully applied of the differential excitation, we introduce it to the wood defect classification.

The definition of differential excitation is shown in (3), where Q represents the pattern parameter. However, the current research only considers the basic case that Q is 8, and the distribution of the position relation between x_c and x_i is shown in Fig. 8-(a). In order to explore the perception model when human eyes observe the target, another seven kinds of positional relation between x_c and x_i are defined as follows. First, the Q patterns of "4+" and "4X" are shown in Figs. 8-(b) and 8-(c) respectively. Second, the Q patterns of "2 |," "2 −," "2 /," and "2\," are shown in Figs. 8-(d) and 8-(g) respectively. In addition, a Q pattern of "6=" is defined as shown in Fig. 8-(f), which is inspired by the ladder-like texture of the crack. It can be seen in Fig. 7,
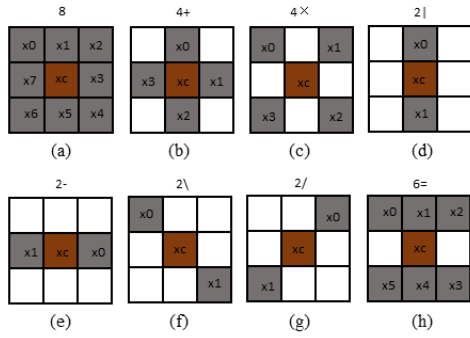
FIGURE 8. Eight patterns of Q: (a) Q ="8," (b) Q ="4+," (c) Q ="4 ×," (d) Q ="2|," (e) Q ="2-," (f) Q ="2\," (g) Q ="2/," and (h) Q ="6=".
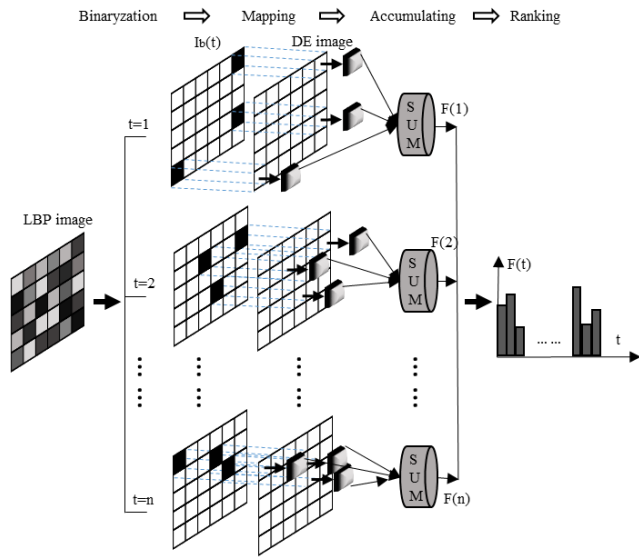

FIGURE 9. Illustration of the basic generating principle of the LB_DEP histogram.

compared with the mineral line, the texture of the crack shows as stair-stepping and each step of the "stair" presents a light-dark-light of the grayscale change in the vertical direction within a local range of 3×3, and the Q pattern of "6=" is established by imitating it. In addition, the effects of total 8 patterns of the Q in Fig. 8 are compared and analyzed in the experimental section.

Based on LBP and DE, a texture description model—LB_DEP is proposed to describe the DE intensity of different textures and the distribution relationship of DE intensity among the textures of an image. And the feature extracted by LB_DEP is expressed in a one-dimensional histogram, called LB_DEP histogram. The basic generating principle of the LB_DEP histogram is shown in Fig. 9. First, the LBP image of the target image area is binary by

$$I_b(x, y) = \begin{cases} 0, & I_{LBP}(x, y) = t \\ 1, & else \end{cases} \quad (6)$$

where I_{LBP} represents the input LBP image, and $I_{LBP}(x, y)$ represents the gray value of pixel position (x, y) in the LBP image. And t is the threshold value, where $0 \le t \le 2^P$-1 and

P represents the number of the LBP sampling points. The I_b represents the output binary image and $I_b(x, y)$ is the gray value of pixel position (x, y) in the image I_b.

Then I_b is mapped to the DE image, and the corresponding DE value $[DE(x, y)]$ of the pixel position (x, y) where $I_b(x, y) = 0$ is calculated. Then, the eigenvalue $F(t)$ of DE is calculated as follows:

$$F(t) = \sum_{(x,y) \in R} DE_t(x, y) \quad (7)$$

where $DE_t(x, y)$ represents the differential excitation value of the pixel position (x, y) where $I_b(x, y) = 0$. And R is the coordinate set which is composed of the pixel positions satisfying $I_b(x, y) = 0$, and t is the threshold value in (6). In the process of taking t from 0 to $(2^P$-1), 2^P $F(t)$ are obtained. Then, the distribution curve generated by the abscissa t and the ordinate $F(t)$ represents the correlation between the texture of the target image area and the DE uniquely. And the distribution curve is the LB_DEP histogram exactly.

C. FEATURE VECTOR GENERATION AND DEFECT CLASSIFICATION

The histograms describing the characteristics of the target image area based on LBP and LB_DEP are obtained above. In this section, the two 1D histograms are fused to generate one 2D histogram as the feature vector which is used to the defect classification with Euclidean distance classifier.

#### 1) METHOD OF GENERATING THE 2D HISTOGRAM

Assume that H_1 and H_2 represent two 1D histograms, and both of which are L in length. The amplitude ranges of the two histograms are $[a_1, b_1]$ and $[a_2, b_2]$ respectively, satisfying $a_1 > a_2$, $b_1 < b_2$. Assume that the ordinal numbers of the points whose value is equal to i in the histogram H_1 construct a set X_i, and the members of X_i are denoted as $X_i(1), X_i(2), \ldots, X_i(|X_i|)$. Where $|X_i|$ is the size of X_i. Then the probability of the occurrence of the data pair (i, j), where j is the value of H_2 at the abscissa X_i, is denoted as

$$P_{ij} = \frac{1}{L} \left\{ n_{ij} | i = H_1(y), j = H_2(X_i), a_1 \le i \le b_1, a_2 \le j \le b_2 \right\} \quad (8)$$

where P_{ij} is a 2D histogram probability function of the image represented by two 1D histograms and n_{ij} is the number of cases that $H_1(y) = i$ and $H_2(X_i) = j$. And y is an independent variable and $a_1 \le y \le b_1$. $H_1(y)$ is the value of the ordinate when the abscissa in histogram H_1 is y. $H_2(X_i)$ is the value of the ordinate when the abscissa in histogram H_2 is X_i. In addition, n_{ij} satisfies

$$\sum_{j=a_2}^{b_2} n_{ij} = |X_i| \quad (9)$$

The above process is shown in Fig. 10. Take the case of the ordinate value H_1 being i as an example, then the ordinate value of $H_2(X_i)$ is marked by the red thick arrows. It can be
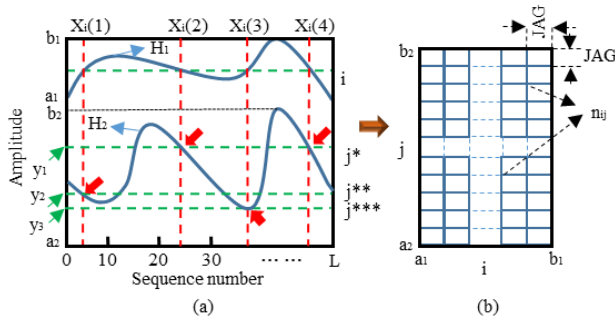
FIGURE 10. Geometrical description of the 2D histogram probability function calculation principle:(a) Probability calculation principle of data pairs (i,j) in 2D histogram, and (b) 2D histograms coordinate plane diagram.
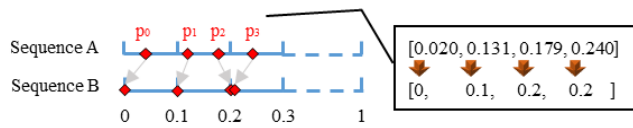
FIGURE 11. Schematic diagram of data consolidation principle.

seen that we get three various effective *j*(marked as j*, j** and j*** respectively in Fig. 10). And when *j* is equal to y_1, n_{ij} is 2 (two red thick arrows). When *j* is equal to y_2, n_{ij} is 1(one red thick arrow). When *j* is equal to y_3, $n_{ij} = 1$ (one red thick arrow). Besides the cases of *j* is y_1, y_2 or y_3, the value of n_{ij} is 0. Consequently, the final 2D histogram coordinate plane has the size of $(b_1-a_1) \times (b_2-a_2)$, and the geometrical description can be shown in the right area of Fig. 10.

2) METHOD OF CONSOLIDATING THE 1D HISTOGRAM

Since the areas of the different defects are various, the amplitudes of the obtained LBP and LB_DEP absolute histograms are various. In order to eliminate the negative effects of the numerical non-equilibrium of two different pattern features on fusion recognition, we first normalize them all. Since there is no negative value in the LBP histogram, it is normalized to 0-1. And the LB_DEP histogram is normalized to -1 to 1 since its absolute histogram has negative values. The specific normalization method is as follows:

$$\xi_n = \xi \,|\, \max_{\xi \in R} \xi \qquad (10)$$

where ξ and ξ_n represent the data before and after normalization respectively, and R represents the set of data to be normalized.

In the right area of Fig. 10, dimension D of the 2D histogram coordinates depends on the interval JAG of i and j. That is, $D =((b_1-a_1)/JAG) \times ((b_2-(a_2))/JAG) = (1/JAG) \times ((1-(-1))/JAG)$, where $0<JAG\leq1$. For example, assume JAG=0.1, then D =10 × 20. And when JAG=0.01, D =100 × 200. However, no matter how much the interval JAG used to establish the 2D histogram is, there will always be the problem that the actual value of the histogram data does not coincide with the sampling point. As shown in Fig. 11,

take 0.1 as the sampling interval, that is $JAG = 0.1$. Then for the sequence A, whose amplitude ranges is from 0 to 1, and the sampling points are 0.1, 0.2, 0.3, ..., 1. But, the values of the data points in sequence A, p_0-p_3, are not multiples of 0.1, which does not coincide with the location of the sampling point. In terms of specific data, a set of possible values of p_0-p_3 are [0.020, 0.131, 0.179, 0.240], and the data cannot be sampled if JAG=0.1. Therefore, before generating the 2D histogram, we first perform an operation of consolidating for the 1D histogram as follows:

$$\begin{cases} v' = \lambda_{low} + (\mu^* \times JAG) \\ \mu^* = \mu \,|\, \min_{\mu=0,1,2,...,\lambda_{high}} \{[\lambda_{low} + (\mu \times JAG)] - v\} \end{cases} \quad (11)$$

where v and v' represent the data before and after consolidation respectively. And JAG represents the sampling interval, λ_{low} and λ_{high} represent the minimum and maximum values of the data sequence to be consolidated respectively. In addition, μ and $\mu*$ are the defined temporary variables.

3) DEFECT IDENTIFICATION

We use Euclidean distance to identify the defects. The specific method is as follows:

$$\begin{cases} E_{ud}(G, \bar{G}_c) < E_{ud}(G, \bar{G}_m), & crack \\ Else, & Mineral lineation \end{cases} \quad (12)$$

where G is an arbitrary 2D histogram which has the same size with $\bar{G}_c$ and $\bar{G}_m$, and $E_{ud}(\cdot, \cdot)$ is defined as

$$E_{ud}(G_1, G_2) = \sqrt{\sum_{u=a_1}^{b_1} \sum_{v=a_2}^{b_2} [G_1(u, v) - G_2(u, v)]^2} \quad (13)$$

In (12), $\bar{G}_c$ and $\bar{G}_m$ represent the reference 2D histogram of the crack and the mineral line respectively, and the calculation is as follows:

$$\begin{cases} \bar{G}_c = \dfrac{1}{p} \sum_{k=1,2,...,p} G_{ck} \\ \bar{G}_m = \dfrac{1}{q} \sum_{k=1,2,...,q} G_{mk} \end{cases} \quad (14)$$

In addition, in (13), $G_1(u, v)$ and $G_2(u, v)$ represent the values of 2D histogram G_1 and G_2 at the coordinate (u, v) respectively. In (14), G_{ck} and G_{mk} represent the 2D histograms of the *k*'th crack and mineral line sample in the training data set, respectively. And p and q represent the total number of the cracks and the mineral lines in the training data set respectively.

Based on the processes above, our algorithm of feature vector generation and the defect classification is implemented by the following steps, as shown in Table 1.

V. EXPERIMENTAL RESULTS AND ANALYSIS

In this section, the proposed wood defect classification algorithm is evaluated. The image data used for the experimental evaluation is established in section III.

TABLE 1. Steps of the proposed feature vector generation and defect classification algorithm.

Step 1	Input: Input the LBP histogram $H(LBP)$ and LB_DEP histogram $H(LB\_DEP)$ of the defect area to be measured.
Step 2	Normalization: Normalize $H(LBP)$ and $H(LB\_DEP)$ and then obtain $N(LBP)$ and $N(LB\_DEP)$ respectively with (10),
Step 3	Consolidation: Step 3.1: Set the sampling interval JAG. Step 3.2: Consolidate $N(LBP)$ and $N(LB\_DEP)$ and then obtain $R(LBP)$ and $R(LB\_DEP)$ respectively with (11),
Step 4	Generation of the 2D histogram: Obtain the 2D histogram feature vector G which is composed of $R(LBP)$ and $R(LB\_DEP)$ based on (8),
Step 5	Matching and recognizing: Input G into (12) for matching and recognizing the defects.

The *Recall*, *Precision*, and False negative rate (*FNR*) are three measurement indexes commonly used to evaluate the performance of the defect detection. The specific definitions are as follows:

$$Recall = \frac{TP}{TP + FN} \tag{15}$$

$$Precision = \frac{TP}{TP + FP} \tag{16}$$

and

$$FNR = \frac{FN}{TP + FN} \tag{17}$$

where *TP* represents the number of the crack samples actually identified as cracks, *FP* represents the number of the crack samples identified as mineral lines, and *FN* represents the number of the mineral lines identified as cracks. To perform the experimental evaluation, a training data set composed of 100 crack areas and 100 mineral line areas in the images is established. These training image areas are used to establish the 1D reference histograms described in section IV-B-1) and the 2D reference histograms described in section IV-C-3). The remaining images which are not used for training in the total data set are used as the testing data set. Thus, the testing data set contains 141 crack defect image areas and 102 mineral line image areas.

In addition, through our observation and statistics about the samples in the data set, the threshold value T in (4) is set to 15, the area value T_a is set to 20, and the threshold of length-width ratio T_r is set to 5. The following experiments are all executed on the basis of the above threshold value of the preprocessing.

A. EVALUATION OF THE LBP CLASSIFICATION EXPERIMENT

In this section, we evaluate the performance of the algorithms in section IV-B-1), and the LBP parameters P and R are set to [8,1] and [16,2] respectively. The performance of the LBP algorithm in our testing data set is shown in Table 2. It can be seen that the parameter [8,1] provides a better performance than the parameter [16,2], but there are still approximately [(141-129)+(102-84)]/(141+102)≈12.3% of the images identified wrongly,

TABLE 2. Comparison of experimental results under different parameters.

Parameters	Correct classification quantity		Recall	Precision	FNR
	Crack	Mineral line			
[8,1]	129	84	0.878	0.915	0.122
[16,2]	106	64	0.736	0.752	0.264
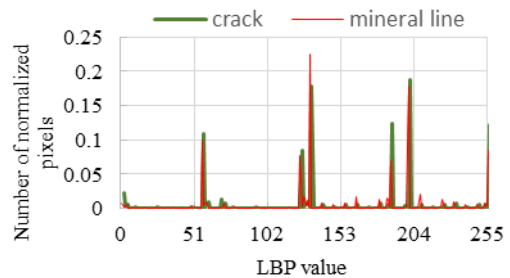
FIGURE 12. Reference LBP histogram based on training data set under parameter [8,1].

especially the mineral line, whose error ratio is about (102-84)/102≈17.6%. Fig. 12 shows the reference histogram obtained from the training data set when the parameter [8,1] is adopted.

B. EVALUATION OF THE LB_DEP CLASSIFICATION EXPERIMENT

Similar to the experimental process in section V-A, the classification effect of LB_DEP is also evaluated by using chi-square distance. The method of obtaining the reference LB_DEP histogram of the cracks and the mineral lines is as the same as (5), which are the average LB_DEP histogram of the cracks and the mineral lines in the training data set respectively. We test the classification algorithm of the LB_DEP in 8 Q patterns in Fig. 8. The reference histograms of the various patterns are shown in Fig. 13, and the performance of LB_DEP of different Q patterns in the testing data set is shown in Fig. 14. It can be seen in Fig. 14 that when Q is "6=," the proposed algorithm obtains the maximum *Recall* and the minimum *FNR*, which is 0.883 and 0.117 respectively. In addition, when Q is "2|," the maximum *Precision* is obtained which is 0.943. In contrast, when Q is "2-," *Recall*, *Precision* and *FNR* all obtain the worst results compared with other Q patterns, indicating that the texture and the distribution pattern of DE of the crack and the mineral line in horizontal direction are very similar. It can be seen from Fig. 8 that the positions of x_i in pattern "2-" and "6=" are complementary. And the results above show that the pattern "6=" which is the pattern "8" removing the position of x_i in the pattern "2-" obtains the best performance. And it also indicates that it is a reasonable and effective way of defining the pattern "6=" based on the characteristic that the crack's texture has a ladder shape.

C. EVALUATION OF THE 2D HISTOGRAM CLASSIFICA-TION ALGORITHM

In section V-A and section V-B, LBP and LB_DEP are evaluated under different parameters respectively. In this section, LBP and LB_DEP are fused, and the parameters prompting

TABLE 3. Performance comparison under various sampling interval JAG of the proposed fusion algorithm.

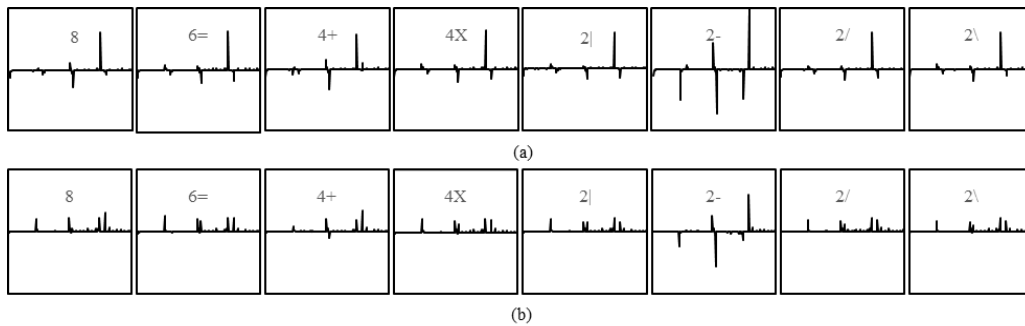| JAG	Eigenvector dimensions	Correct classification quantity		Recall	Precision	FNR
		Crack	Mineral line			
0.01	100×200	109	79	0.826	0.773	0.174
0.02	50×100	118	86	0.881	0.837	0.119
0.05	20×40	133	92	**0.930**	**0.943**	**0.070**
0.1	10×20	126	87	0.894	0.894	0.106
0.2	5×10	125	83	0.868	0.887	0.132
0.5	2×4	127	77	0.836	0.901	0.164
1	1×2	122	58	0.735	0.865	0.265

FIGURE 13. LB_DEP reference histograms of various Q patterns: (a) Crack reference histograms and (b) Mineral line reference histogram.
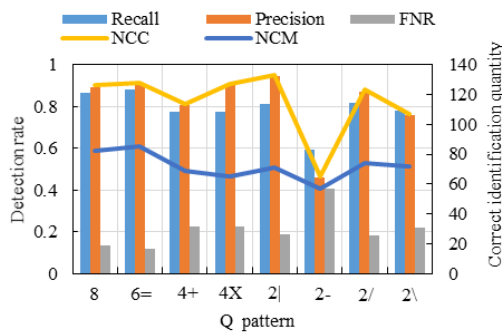

FIGURE 14. Classification performance of the proposed LB_DEP algorithm in various Q patterns. "NCC" and "NCM" represent the number of the correctly identified cracks and mineral lines respectively.

the algorithm of LBP and LB_DEP obtain the optimum performance respectively are selected. Finally, the parameters P and R of the LBP algorithm are selected [8, 1], and the parameter Q of the LB_DEP algorithm is selected "6=." It should be noted that the highest *Recall* and *Precision* in section V-B belong to two different groups. Since *Recall* reflects the comprehensive performance of the algorithm, we chose the pattern "6=" to conduct the fusion experiments.

In the process of generating 2D histograms from the obtained 1D histograms of LBP and LB_DEP, the sampling interval *JAG* will affect the precision of the coordinate system of the 2D histogram. Consequently, the dimension of the feature vectors which directly reflects the richness of the feature information is affected also, and then it has great

impact on the defect identification. Therefore, we perform the comparison experiment under different sampling interval *JAG*, and the results are shown in Table 3. The value of *JAG* is selected based on the principle that the data in the 1D histogram can be sampled at equal intervals, that is to say, the dimension of the 2D eigenvector should be guaranteed to be an integer. It can be seen from Table 3 that when *JAG* = 0.05, the algorithm achieves the highest *Recall* of 0.930 and *Precision* of 0.943, and the lowest *FNR* of 0.070. Compared with the best results by using LBP or LB_DEP solely on the testing data set, the fusion algorithm achieves better performance, indicating that the proposed algorithm could provide a robust descriptor for the classification of the wood defects.

Fig. 15 shows the 2D histogram of the crack and the mineral line in the testing data set when *JAG* = 0.05. Fig. 16 shows the reference 2D histogram when *JAG* = 0.05. The reason of the algorithm can achieve the best performance when *JAG* = 0.05 is analyzed as follows. The smaller the *JAG* is, the more sampling points there are, and the more elaborate the description of the target image texture is. Since the more elaborate the description is, the more powerful it is to express the unique characteristics of each texture, and the more powerful it is to magnify the differences of the similar textures consequently. Thus, the similarity of the similar textures is reduced further, which will lead to false rejection easily. In contrast, the larger the *JAG* is, the fewer the sampling points are, and the rougher the description of the target image texture is. And when its roughness exceeds
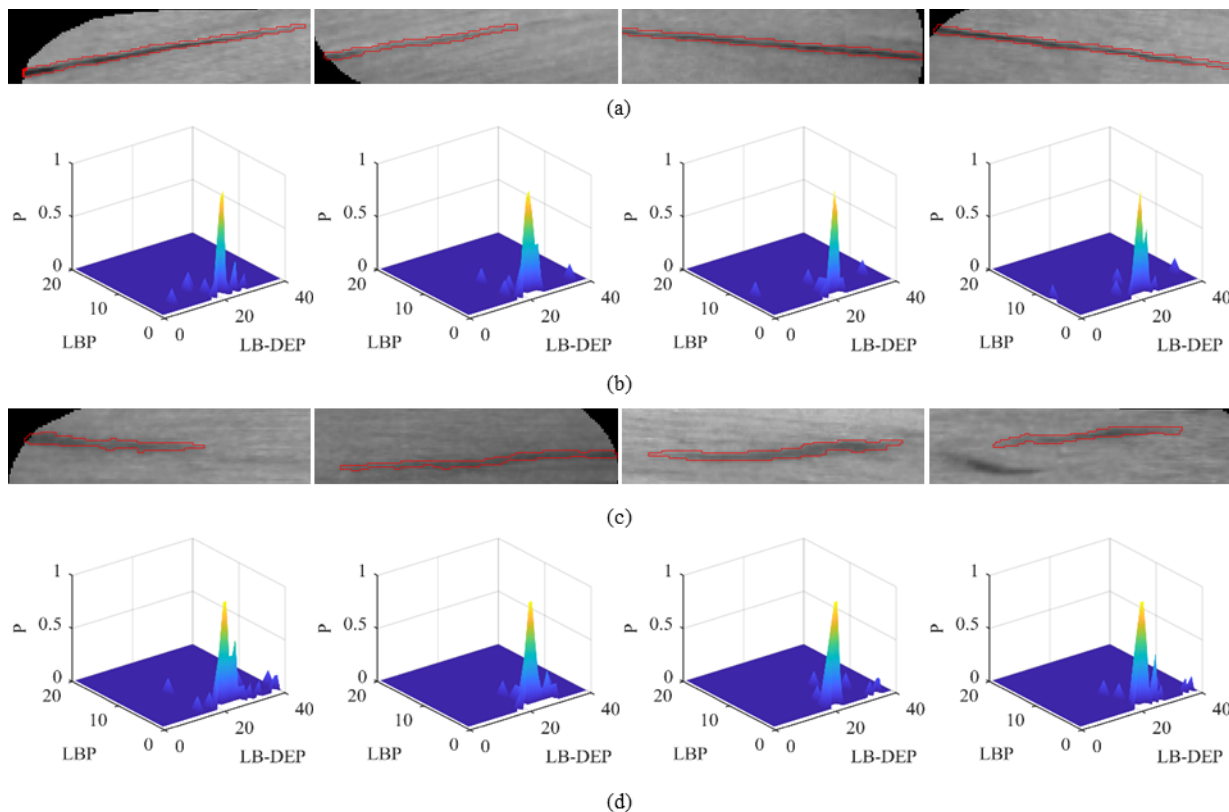
FIGURE 15. 2D histogram of the crack and mineral line in the testing data set, *JAG*=0.05: (a) Crack images and the segmentation effect, (b) 2D histogram of the crack areas, (c) Mineral line images and the segmentation effect, and (d) 2D histogram of the mineral line areas.

a certain value, it is difficult to distinguish two different textures.

Furthermore, we observe the wrongly judged samples, and the typical representatives are shown in Fig. 17. The cracks misjudged could be divide into two categories. For the first category, as shown in Fig. 17-(a), the image texture inside the crack area is blurred, which may be caused by the poor imaging effect, and it results in the losing of effective texture characteristics. Consequently, it leads to the wrong judgment. The second category is the discontinuous cracks as shown in Fig. 17-(b). It can be seen that in the linear crack area, the cracks on the left and right sides are more obvious, and a gap appears in the middle. Therefore, when the gap is taken as the target to extract the features, the degree of the ''crack attribute'' on the left and right side is pulled down by the middle, resulting in the wrong judgment. The distribution of the categories and quantities of the misjudged cracks in the testing data set is shown in Fig. 18-(a).

According to the observation of the misjudged mineral lines in the testing data set, the texture distribution and grayscale contrast are very similar to the crack, as shown in Fig. 17-(c). It is because that the mineral pigment deposition has a certain degree of randomness. In addition, we have observed that the average width of these misjudged mineral lines is smaller. Fig. 18-(b) shows the average width distribution of the misjudged mineral lines in the testing data set.

It can be seen that the width of all of them are less than 5 pixels, and most of them are only 2 pixels. But according to the prior knowledge, the average width of the mineral lines in the data set is 6 pixels wide. The reason is that the smaller the width of the mineral line is, the less the possible of the pigment random distribution is.

Fig. 19 shows the curve of the time consumption of the 2D histogram generation algorithm and the Euclidian distance classification algorithm under various value of *JAG*. It can be seen that as the value of *JAG* increases, the time consumption of the algorithm decreases exponentially approximately. It is because that the dimension of the eigenvector decreases exponentially as the value of *JAG* increases, and the specific data of the eigenvector dimensions are shown in Table 2. And it also can be seen that when $JAG = 0.05$, the algorithms take less than 0.1 s.

D. COMPARISON OF THE CLASSIFICATION PERFORMANCE

To illustrate the classification performance of the algorithm we proposed, it is compared with LSURF [13], GLCM, LGLCM [24], etc. The LSURF combines LBP with SURF, which is the method in [13]. The GLCM extracts 5 typical gray level co-occurrence matrix features of the image area to be tested, and then classifies the image area with
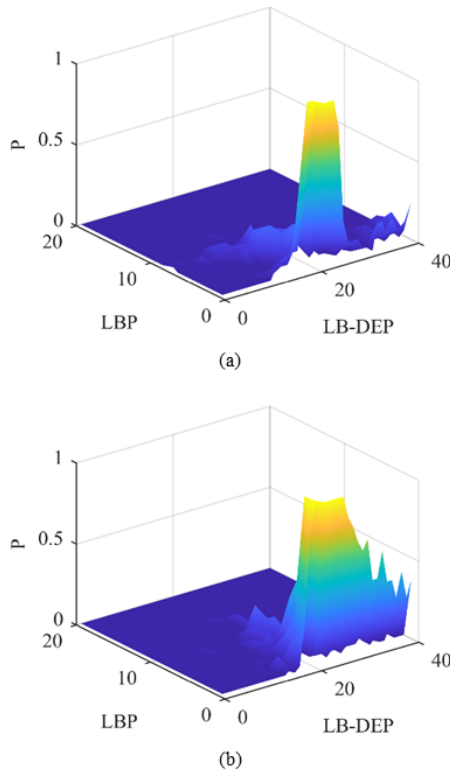
(a)

(b)

FIGURE 16. 2D reference histograms of the crack and the mineral line generated from the training data set, *JAG*=0.05: (a) Crack 2D reference histograms and (b) Mineral line 2D reference histograms.
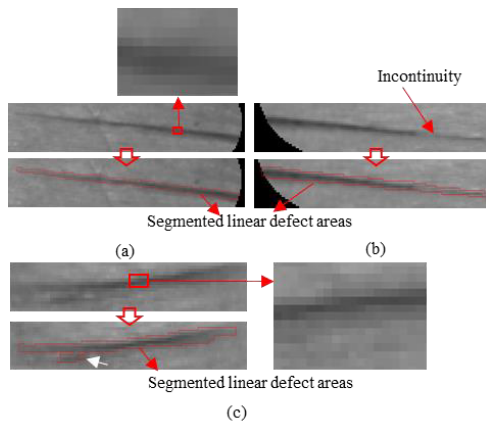

FIGURE 17. Misjudged samples in the testing data set: (a) Blurred crack, (b) Discontinuous crack and (c) Mineral line.

Euclidean distance. The LGLCM is the combination of LBP and GLCM, which is the method in [24]. GLTA is the combination of GLCM and TAMURA, it is a feature combination method for wood surface defect classification proposed in [45]. And in this experiment, we extract 5 typical features of GLCM and 6 feature components of TAMURA, and then use Euclidean distance to classify the defects. The method of GF extracts 17 grayscale features in [15], and then Euclidean distance is used to classify the defects. In addition, we also compare the sub-region variable-scale Gaussian
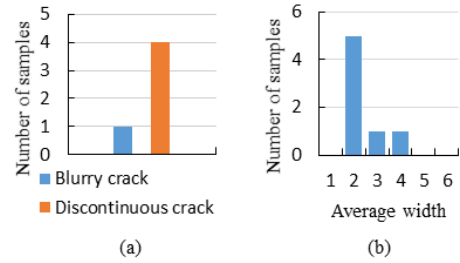

FIGURE 18. Parameter distribution of the misjudged samples in the testing data set: (a) Crack and (b) Mineral line.
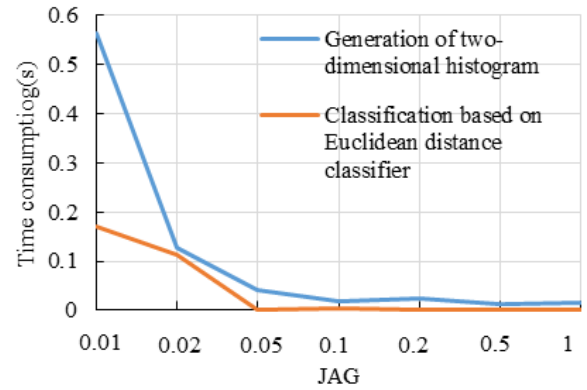

FIGURE 19. Distribution trend of the time consumption of the algorithms we proposed under different *JAG*.

TABLE 4. Effect comparison between the method we proposed and other methods.

Methods	Recall	Precision	FNR	Time consumption(s)
The method we proposed	0.930	0.943	0.070	0.1416
LSURF [13]	0.915	0.915	0.085	0.1840
LGLCM [24]	0.928	0.908	0.072	0.0922
GLTA [45]	0.852	0.858	0.148	0.0798
TRF [19]	0.887	0.894	0.113	0.0259
SRVSG [18]	0.871	0.865	0.129	0.0391
GF [15]	0.826	0.809	0.174	0.0522
GLCM[23]	0.791	0.780	0.209	0.0572

TABLE 5. Time consumption of the proposed algorithm in this research.

Algorithm process	Time consumption(s)
LBP histogram generation	0.0423
LB_DEP histogram generation	0.0549
2D histogram generation	0.0426
Euclidean distance calculation	0.0018

fitting method (SRVSG) [18] and the texture ridge feature method (TRF) [19] previously proposed by our research group.

Table 4 shows the comparison performance between our method proposed in this research and the other state-of-the-art methods mentioned above. It can be seen that our

method obtains better results in *Recall*, *Precision* and *FNR* compared with the others. In terms of the time consumption, our method and the other methods are all at the millisecond level. Table 5 shows the time consumption of the each process of our algorithm. And the results of the process "2D histogram generation" and "Euclidean distance calculation" are calculated when $JAG = 0.05$.

VI. CONCLUSION

This paper has presented a defect classification algorithm of birch veneer surface. First, an imaging equipment has been constructed to capture the images of the upper and lower surface of the birch ice cream bar, and then the image data set which includes the crack and mineral line is established. On the basis of LBP and Weber's law, we propose a LB_DEP descriptor for describing the incidence relation between the image texture and the human visual perception. Then we establish a 2D histogram based on the LBP 1D histogram and the LB_DEP 1D histogram after being normalized and consolidated. Euclidean distance classifier is used for the defect classification with the extracted 2D histogram feature. We conduct the experiments to evaluate our proposed algorithm. The results have demonstrated that the proposed algorithm can provide a better classification effect for the crack and the mineral line of the birch ice cream bar— the *Recall*, *Precision* and *FNR* are 0.930, 0.943 and 0.070 respectively. In addition, the average time consumption of the algorithm in the testing data set is 0.1416 s, which belongs to the millisecond level as with the compared state-of-the-art methods. In future work, we plan to apply this algorithm to other data sets, as well as other category of defects, such as the knot defect and the contamination defect.
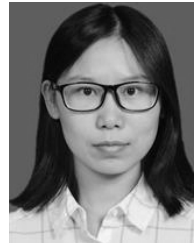
ACKNOWLEDGMENT

REFERENCES

[1] H. Mu, M. Zhang, D. Qi, and H. Ni, "The application of RBF neural network in the wood defect detection," *Int. J. Hybrid Inf. Technol.*, vol. 8, no. 2, pp. 41–50, 2015.

[2] L. Lin, S. He, F. Fu, and X. Wang, "Detection of wood failure by image processing method: Influence of algorithm, adhesive and wood species," *Eur. J. Wood Wood Products*, vol. 73, no. 4, pp. 485–491, 2015.

[3] W. S. Lin and J. Z. Wu, "Study on application of stress wave for non-destructive test of wood defects," *Appl. Mech. Mater.*, vols. 401–403, pp. 1119–1123, Sep. 2013.

[4] J. Sun, Y. Hu, and F. Wang, "Study on quantitative nondestructive test of wood defects based on intelligent technology," *Chin. J. Sci. Instrum.*, vol. 34, no. 9, pp. 1955–1960, 2013.

[5] M. C. Di Tuccio, N. Ludwig, M. Gargano, and A. Bernardi, "Thermographic inspection of cracks in the mixed materials statue: Ratto delle Sabine," *Heritage Sci.*, vol. 3, no. 1, p. 10, 2015.

[6] Z.-N. Ke, Q.-J. Zhao, C.-H. Huang, P. Ai, and J.-G. Yi, "Detection of wood surface defects based on particle swarm-genetic hybrid algorithm," in *Proc. Int. Conf. Audio, Lang. Image Process.*, Jul. 2016, pp. 375–379.

[7] Y. Zhang, C. Xu, C. Li, H. Yu, and J. Cao, "Wood defect detection method with PCA feature fusion and compressed sensing," *J. Forestry Res.*, vol. 26, no. 3, pp. 745–751, Mar. 2015.

[8] Y. Z. Zhang, L. Xu, L. Ding, and J. Cao, "Defects segmentation for wood floor based on image fusion method," *Electr. Mach. Control*, vol. 18, no. 7, pp. 113–118, 2014.

[9] L. Chao, Y. Zhang, W. Tu, C. Jun, H. Liang, and H. Yu, "Soft measurement of wood defects based on LDA feature fusion and compressed sensor images," *J. Forestry Res.*, vol. 28, no. 6, pp. 1285–1292, 2017.

[10] Z. Chang, J. Cao, and Y. Zhang, "A novel image segmentation approach for wood plate surface defect classification through convex optimization," *J. Forestry Res.*, vol. 29, no. 6, pp. 1789–1795, 2018.

[11] D.-Y. Wu, N. Ye, L.-R. Shen, Q.-Q. Zhang, and Z.-W. Lai, "Clustering method for automatic timber defects detection based on the color moment," *J. Jiangnan Univ. (Natural Sci. Ed.)*, vol. 8, no. 5, pp. 520–524, 2009.

[12] D. Wu, N. Ye, and X. Su, "Wood defect recognition based on GLCM and clustering algorithm," *Comput. Digit. Eng.*, vol. 38, no. 11, pp. 38–41, 2010.

[13] M. M. Hittawe, S. M. Muddamsetty, D. Sidibé, and F. Mériaudeau, "Multiple features extraction for timber defects detection and classification using SVM," in *Proc. IEEE Int. Conf. Image Process.*, Sep. 2015, pp. 427–431.

[14] S. Shnhnorbanun, "A computational biological network for wood defect classification," *Lect. Notes Eng. Comput. Sci.*, vol. 2186, no. 1, pp. 559–563, 2010.

[15] D. Drake and M. S. Packianather, "A decision tree of neural networks for classifying images of wood veneer," *Int. J. Adv. Manuf. Technol.*, vol. 14, no. 4, pp. 280–285, 1998.

[16] M. S. Packianather, P. R. Drake, and D. T. Pham, "Feature selection method for neural network for the classification of wood veneer defects," in *Proc. IEEE Autom. Congr.*, Sep./Oct. 2008, pp. 1–6.

[17] Y. Baris, E. Mastrocinque, M. S. Packianather, D. Pham, A. Lambiase, and F. Fruggiero, "Neural network design and feature selection using principal component analysis and Taguchi method for identifying wood veneer defects," *Prod. Manuf. Res., Open Access J.*, vol. 2, no. 1, pp. 291–308, 2014.

[18] W. Yuan, S. Li, and D. Li, "Wood surface defect recognition based on sub-region zoom Gaussian fitting," *Chin. J. Sci. Instrum.*, vol. 37, no. 4, pp. 879–886, 2016.

[19] W. Yuan, S. Li, and D. Li, "Wood surface crevice detection based on fusion of texture ridge line features," *Chin. J. Sci. Instrum.*, vol. 38, no. 2, pp. 436–444, 2017.

[20] T. Ojala, M. Pietikainen, and M. Mäenpää, "Multiresolution gray-scale and rotation invariant texture classification with local binary patterns," *IEEE Trans. Pattern Anal. Mach. Intell.*, vol. 24, no. 7, pp. 971–987, Jul. 2002.

[21] T. Ojala, M. Pietikäinen, and D. Harwood, "A comparative study of texture measures with classification based on featured distributions," *Pattern Recognit.*, vol. 29, pp. 51–59, Jan. 1996.

[22] Y. F. Zheng, Q. R. Zhang, and Z. Zhang, "Damped Newton based iterative non-negative matrix factorization for intelligent wood defects detection," *J. Softw.*, vol. 5, no. 8, pp. 899–906, 2010.

[23] K. Kobayashi, S.-W. Hwang, T. Okochi, W.-H. Lee, and J. Sugiyama, "Non-destructive method for wood identification using conventional X-ray computed tomography data," *J. Cultural Heritage*, vol. 38, pp. 88–93, Jul. 2019.

[24] H. Kuang, Y. Ding, R. Li, and X. Liu, "Defect detection of bamboo strips based on LBP and GLCM features by using SVM classifier," in *Proc. 30th Chin. Control Decis. Conf. (CCDC)*, Jun. 2018, pp. 3341–3345.

[25] P. Amorim, T. Goudon, and F. Peruani, "An ant navigation model based on Weber's law," *J. Math. Biol.*, vol. 78, no. 4, pp. 943–984, 2019.

[26] V. M. K. Namboodiri, S. Mihalas, and M. G. H. Shuler, "Analytical calculation of errors in time and value perception due to a subjective time accumulator: A mechanistic model and the generation of Weber's law," *Neural Comput.*, vol. 28, no. 1, pp. 89–117, 2016.

[27] G. Zhu, S. Zhang, X. Chen, and C. Wang, "Efficient illumination insensitive object tracking by normalized gradient matching," *IEEE Signal Process. Lett.*, vol. 14, no. 12, pp. 944–947, Dec. 2007.

[28] B. Wang, W. Li, W. Yang, and Q. Liao, "Illumination normalization based on Weber's law with application to face recognition," *IEEE Trans. Signal Process. Lett.*, vol. 18, no. 8, pp. 462–465, Aug. 2011.

[29] J. Chen, S. Shan, C. He, G. Zhao, M. Pietikainen, X. Chen, and W. Gao, "WLD: A robust local image descriptor," *IEEE Trans. Pattern Anal. Mach. Intell.*, vol. 32, no. 9, pp. 1705–1720, Sep. 2010.

[30] R. Lv, Z.-H. Xia, X.-Y. Chen, and X.-M. Sun, "Fingerprint liveness detection based on weber binarized perception features," *J. Appl. Sci.*, vol. 34, no. 5, pp. 616–624, 2016.

[31] C. Qin, Y. Hu, H. Yao, X. Duan, and L. Gao, "Perceptual image hashing based on weber local binary pattern and color angle representation," *IEEE Access*, vol. 7, pp. 45460–45471, 2019.

[32] D. Tiwari and V. Tyagi, "Improved Weber's law based local binary pattern for dynamic texture recognition," *Multimedia Tools Appl.*, vol. 76, no. 5, pp. 6623–6640, 2017.

[33] Y. Chen, "No-reference image quality assessment based on differential excitation," *Acta Automat. Sinica*, to be published. doi: 10.16383/j.aas. c180088.

[34] F. Liu, Z. Tang, and J. Tang, "WLBP: Weber local binary pattern for local image description," *Neurocomputing*, vol. 120, pp. 325–335, Nov. 2013.

[35] Y. T. Luo, L. Y. Zhao, and W. Jia, "Palmprint recognition method based on line feature Weber local descriptor," *J. Image Graph.*, vol. 21, no. 2, pp. 235–244, 2016.

[36] H. Fan, F. Xie, Y. Li, Z. Jiang, and J. Liu, "Automatic segmentation of dermoscopy images using saliency combined with Otsu threshold," *Comput. Biol. Med.*, vol. 85, pp. 75–85, Jun. 2017.

[37] J.-H. Seong and D.-H. Seo, "Wi-Fi fingerprint using radio map model based on MDLP and Euclidean distance based on the Chi squared test," *Wireless Netw.*, vol. 25, no. 6, pp. 3019–3027, 2018.

[38] Z. Guo and D. Zhang, "A completed modeling of local binary pattern operator for texture classification," *IEEE Trans. Image Process.*, vol. 19, no. 6, pp. 1657–1663, Jan. 2010.

[39] L. Liu, P. Fieguth, Y. Guo, X. Wang, and M. Pietikäinen, "Local binary features for texture classification: Taxonomy and experimental study," *Pattern Recognit.*, vol. 62, pp. 135–160, Feb. 2017.

[40] L. Zhang, L. Zhang, and A. C. Bovik, "A feature-enriched completely blind image quality evaluator," *IEEE Trans. Image Process.*, vol. 24, no. 8, pp. 2579–2591, Apr. 2015.

[41] Y. F. Lu, T. Zhang, and C. Zhang, "Image quality assessment using log-Gabor Weber feature," *Opt. Precis. Eng.*, vol. 23, no. 11, pp. 3259–3269, 2015.

[42] S. Lee and J. Kim, "Vessel pattern enhancement based on Weber's law for sclera recognition," in *Proc. Int. Conf. Electron., Inf., Commun. (ICEIC)*, Jan. 2018, pp. 1–2.

[43] Y. Wang, M. Pomeroy, W. Cao, Y. Gao, E. Sun, S. Stanley, III, J. C. Bucobo, and Z. Liang, "Polyp classification by Weber's Law as texture descriptor for clinical colonoscopy," *Proc. SPIE*, vol. 10950, Mar. 2019, Art. no. 109502V.

[44] M. Tian and X. L. Hao, "Facial expression recognition based on binary Weber local descriptor and deep belief net," *Comput. Eng. Des.*, vol. 39, no. 2, pp. 542–546, 2018. doi: 10.16208/j.issn1000-7024.2018.02.044.

[45] X. YongHua and W. Jin-Cong, "Study on the identification of the wood surface defects based on texture features," *Optik-Int. J. Light Electron Opt.*, vol. 126, no. 19, pp. 2231–2235, Oct. 2015.

SHAOLI LI received the B.S. and Ph.D. degrees from the School of Information Science and Engineering, Shenyang University of Technology, Shenyang, China, in 2013 and 2018, respectively, where she is currently a Researcher with the Electrical Engineering Postdoctoral Research Station. At the same time, she is a member of the Computer Vision Group, Shenyang University of Technology. In recent years, she published more than ten technical articles. Her current research interests include machine vision, image processing, and industrial product quality inspection.

DEJIAN LI received the B.S. and Ph.D. degrees from the School of Information Science and Engineering, Shenyang University of Technology, Shenyang, China, in 2013 and 2018, respectively, where he is currently a Researcher with the Electrical Engineering Postdoctoral Research Station. His current research interests include machine vision and biometric identification.

WEIQI YUAN received the B.S. degree from Hunan University, Changsha, China, in 1982, and the M.S. and Ph.D. degrees from Northeastern University, Shenyang, China, in 1988 and 1997, respectively.

He is currently a Professor with the Shenyang University of Technology. He is also the Executive Director of the Chinese Instrument Association and the Director of Biomedical Electronics Branch of the Chinese Electronics Association. In recent years, he published more than 100 technical articles and has authored one book. He holds six patents. His current research interests include machine vision, biometric identification, and nondestructive testing. In 2000, he was selected to the second batch of "hundreds of thousands of talents project" by Liaoning, China. In 2001, he was awarded the title of "outstanding scientific and technological workers of Shenyang" by Shenyang municipal party committee and Shenyang municipal government. In 2003, he was selected as "senior software talents of Shenyang".

● ● ●